Report Number: WUCS-96-01

1996-01-01

# Analysis of MPEG Compressed Video Traffic

Jerome R. Cox Jr. and O. Matthew Beal

This paper outlines a study of MPEG compressed video sequences and simulation of multiplexed video traffic in the ATM environment. A number of statistical characteristics including autocorrelation and variance of MPEG-1 compressed video sequences are used to characterize the 16 sample traces used in this study. From these measurements, a preliminary model is developed which utilizes basic measurements of the individual component video sequences to predict bandwidth requirements and cell loss of the multiplexed video traffic.

# Analysis of MPEG Compressed Video Traffic

Jerome R. Cox, Jr. and O. Matthew Beal

WUCS 96-01

January 1996
Revised: August 1996

Department of Computer Science
Applied Research Laboratory
Campus Box 1045
Washington University
One Brookings Drive
St. Louis, MO. 63130-4899

## Abstract

This paper outlines a study of MPEG compressed video sequences and simulation of multiplexed video traffic in the ATM environment. A number of statistical characteristics including autocorrelation and variance of MPEG-1 compressed video sequences are used to characterize the 16 sample traces used in this study. From these measurements, a preliminary model is developed which utilizes basic measurements of the individual component video sequences to predict bandwidth requirements and cell loss of the multiplexed video traffic.

# Table of Contents



# Appendices

# List of Figures



# List of Tables

# 1. Introduction

Advances in network technology offer new opportunities for multimedia communications systems which were not possible in the past. Much attention has been given to research into the many issues which will affect multimedia communications, especially video transmission and distribution. Buzz words like interactive television and video-on-demand services have become commonplace in these discussions. However, to make such services possible, the manner in which video will be incorporated into the network environment must first be determined [32]. One of the primary issues which must be understood before this is possible is how large scale video transmission will affect the network [31]. Models of cell loss, delay and other critical factors must be derived.

Recent research has shown that variable bit rate (VBR) video sources show significant long-term and self-similar behavior [1,4,5]. This increases the already complex development of statistical models which are robust enough to accurately predict the behavior of video traffic in the ATM network. In this study, a video distribution methodology will be described. The nature and behavior of 16 MPEG coded video sequences will be explored using estimates of autocorrelation, variance and distribution. Additionally, a number of different traffic simulations using these sample MPEG video sources will be presented. A preliminary model will then be developed which will predict the behavior of MPEG traffic in the ATM environment. This model provides a means of predicting the cell loss of the aggregate traffic using three simple measurements from each component of the aggregate traffic.

# 2. Proposed Video Distribution

Video distribution in the ATM environment is likely to be deployed in a number of configurations. However, this work focuses on the configuration illustrated in Fig. 1. The multimedia server below feeds a number of video streams into a multiplexor which then relays the multiplexed aggregate video stream to the ATM network via a single link. The individual video streams are then broadcast through the ATM network to a number of home receivers, enabling video-on-demand and other interactive television services.

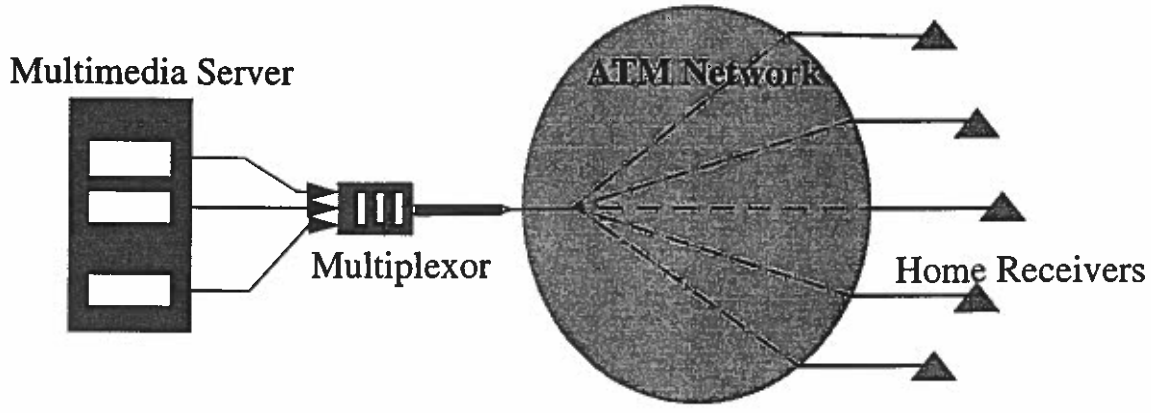


*Figure 1: Video Distribution Schematic*

In a configuration similar to the one shown in Fig. 1, a transmission bottleneck is expected at the link between the network and the multiplexor. To plan for efficient usage of network resources, the number of video sources which can be sent reliably across a single link must be computed. In order to compute the expected number of video sources which can be broadcast across a single link, the statistical nature of the video traffic must be understood.

## 3. MPEG Image Coding Basics

The MPEG (Moving Pictures Expert Group) compression algorithm is a standard jointly developed by the International Organization of Standards (ISO) and the International Electrotechnical Commission (IEC). The MPEG algorithm utilizes the Discrete Cosine Transform (DCT) and motion entropy coding to obtain extremely high compression ratios [12]. For this project, a sample set of sixteen MPEG-1 compressed video sequences were studied to evaluate a number of measurement and traffic simulation techniques.

MPEG compressed video streams are composed of a number of hierarchical elements [13]. The highest layer is the Sequence layer. This layer is made up of an arbitrary number of Groups of Pictures (GOPs). In turn, each GOP is made up of a number of frames.

The MPEG compression standard defines three frame types. The first frame type is the Intra- or I frame. This frame is coded with reference to the current frame only. The second frame type, the Predictive or P frame differs from the I frame in that it is coded with reference to the current frame and a previous I or P frame. The third frame type, the Bidirectional or B frame, is even more complex because it is coded with reference to a past and a future I or P frame as well as the current frame. These complex interrelationships are shown in Fig. 2.

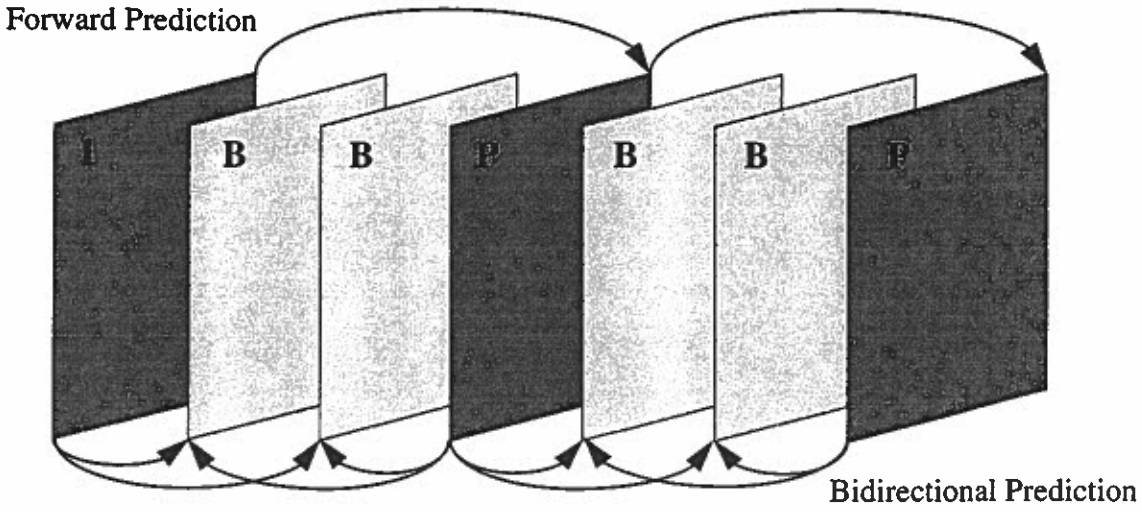


*Figure 2: MPEG Frame Level Structure*

Each frame consists of one or more slices which are made up of groups of macroblocks (MBs). Motion compensation information is contained in the macroblock layer. Below the macroblock

layer is the final layer, the block layer, which contains the DCT coded image data [8,9].

In this study, the GOP and Frame layers will be considered, but this work will concentrate on the GOP layer, primarily due to the findings in the following section.

## 4. GOPs and Frames as Network Traffic

A rudimentary method of evaluating the burstiness of MPEG streams in the ATM network is to compare frame and GOP size traces for a number of video sequences. The frame and GOP size traces shown in Fig.3 are representative of the 16 MPEG-1 sample traces used in this study. The trace with the greater magnitude is the GOP size trace and the trace with the lesser magnitude is the frame size trace. The solid horizontal lines represent the average of the respective trace while the dashed lines indicate values one standard deviation from the average value. The regularly dashed line corresponds to one standard deviation above average while the irregularly dashed line corresponds to one standard deviation below average. (The irregularly dashed line for the frame trace is not shown because it is below zero.)

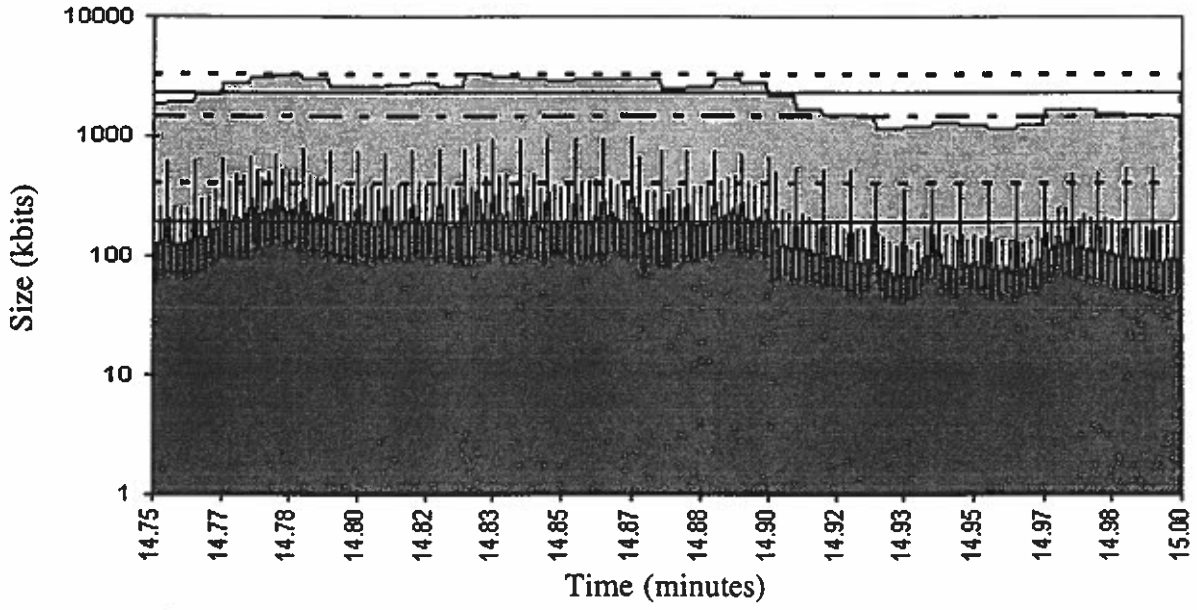


***Figure 3: GOP and Frame Size Trace from Bond***

As can be seen in Fig. 3, the relative variance between GOPs is less than that for frames, giving a visual idea of the traffic's burstiness. This rudimentary estimation of burstiness at the frame level versus that at the GOP level provides insight into one method of incorporating MPEG video traffic into the ATM network. By smoothly pacing MPEG traffic out of the server at the GOP level, the burstiness of the traffic can be reduced. This provides a means of implementing VBR video in the ATM environment which offers promising statistical multiplexing gains without the extreme burstiness of frame level traffic.

## 5. GOP Size Distribution

However, the feasibility of broadcasting MPEG video streams by transmitting ATM cells which are smoothly paced through a GOP must be evaluated. Two important criteria must be met before this method can be deemed acceptable. First, GOP level transmission cannot introduce unacceptable transmission delays. Second, the buffer size at the decoder should not be increased significantly. If either of these two requirements cannot be met, this method may prove to be too inefficient or too expensive.

Given a buffer with adequate size to store an entire GOP, the first criteria can be met by pacing the GOPs from the server at a rate which will ensure that the decoder will have a complete compressed GOP in the buffer at the time it completes decoding of the previous GOP. The size required by the buffer must therefore be large enough to allow for decompression of the video frames as well as to store a full GOP.

To provide adequate memory for decoding, the buffer must be large enough to store a minimum of two decompressed video frames. The reason for this is that to decode a B frame, the preceding and succeeding I or P frames must first be decoded and retained in memory. This data will be used with the appropriate prediction information to decode the full B frame.

By studying the histogram of GOP sizes shown in Fig. 4, an estimate of the buffer size required to store a compressed GOP can be calculated.

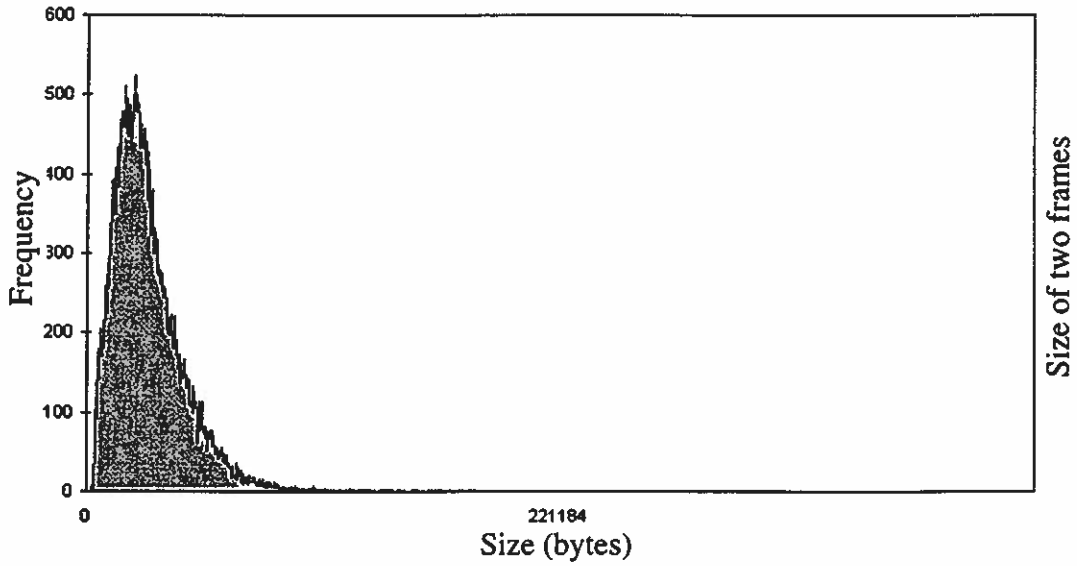


*Figure 4: Histogram of GOP Sizes*

For this study, the frame size was set at 288 lines of 384 pixels each, or 110,592 pixels. This requires 221,184 bytes (YUV 4:2:2) to represent each frame. A buffer which is capable of storing two frames will therefore require 442,368 bytes of memory. From the above histogram, a GOP size estimate of approximately half the size required to store a single decoded frame will

accommodate almost all of the GOPs in the sample set. This estimate results in a calculation of 552,960 bytes. From this estimate, the buffer required to broadcast the MPEG-1 video streams used in this study will be only 25% greater than the buffer size required for decoding (the size of two decompressed frames).

## 6. Development of Sample Set

Before proceeding with this discussion, a brief description of the sample set used in this study is required. To this point, 16 different video traces have been considered. The subject matter of the traces includes movies, cartoons, and sports. Each trace is the same length, 40000 frames, and is digitized at a resolution of 384 by 288 pixels per frame. This translates to roughly 27 minutes of video per trace [28].

The GOP parameters used to encode the video sequences were set at a GOP size of 12 with a GOP structure of IBBPBBPBBPBB. The MPEG quantizer scales were set at 10 for the I frames, 14 for the P frames, and 18 for the B frames. Each frame consists of one slice and the macroblocks are encoded using a logarithmic motion vector search.

Physically, the video sequences were created using the scheme shown in Fig. 5 by Oliver Rose at the University of Wuerzburg [28]. Because of the complexity of MPEG encoders, real-time encoders remain expensive and not widely available. Due to this fact, digitization and compression were performed separately. A Sun Sparc 20 equipped with a SunVideo card was used to digitize the analog video from the VCR. After the video was digitized, the UC Berkeley MPEG-1 software encoder was used to create the MPEG video stream.

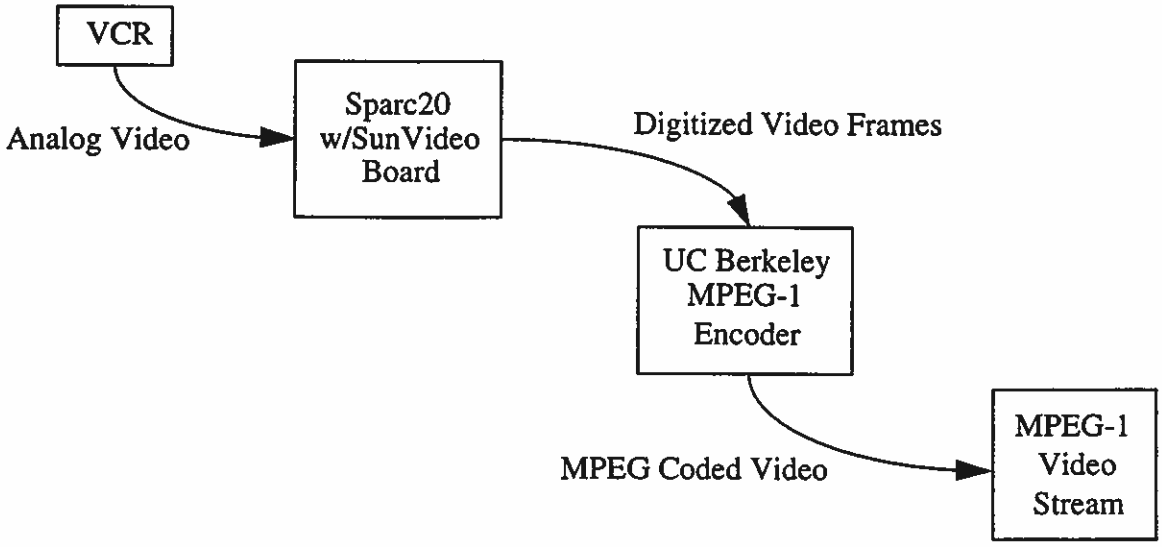


***Figure 5: MPEG Encoding Process***

After the compressed MPEG streams were computed, frame size traces were calculated from the number of bits required to store each compressed frame. This information became the foundation for the statistical analysis of this study.

## 7. Basic Statistical Profile of Video Sequences

To better understand the nature of the 16 MPEG coded video sequences used in this study, a number of basic measurements were made. These measurements include the length of each video sequence, the average size of each GOP in both bytes and bits per pixel, and the peak to average ratio at both the frame level and the GOP level. Table 1 below lists these measurements as well as other information for each of the video sequences.

**Table 1: Basic Characteristics of 16 MPEG-1 Video Sequences**

| Brief Name | Full Name | Subject | Length (MBytes) | Avg. GOP Size (kbytes) | Avg. GOP Size (bits/pixel) | GOP Peak/Avg. Ratio | Frame Peak/Avg. Ratio |
|---|---|---|---|---|---|---|---|
| ast | Asterix | cartoon | 112 | 34 | 0.2021 | 4.02 | 6.59 |
| bond | James Bond | movie | 122 | 36 | 0.2198 | 3.28 | 10.06 |
| jp | Jurassic Park | movie | 65 | 20 | 0.1183 | 4.00 | 9.15 |
| mtv1 | MTV clip 1 | television | 123 | 37 | 0.2225 | 4.34 | 9.32 |
| mtv2 | MTV clip 2 | television | 99 | 30 | 0.1789 | 6.14 | 12.71 |
| news1 | News clip | television | 77 | 23 | 0.1389 | 6.05 | 12.36 |
| race | Formula 1 car race | sports | 154 | 46 | 0.2780 | 3.61 | 6.58 |
| lambs | Silence of the Lambs | movie | 37 | 11 | 0.0661 | 5.27 | 18.36 |
| simp | Simpsons | cartoon | 93 | 28 | 0.1680 | 3.76 | 12.94 |
| soccer1 | Soccer clip 1 | sports | 136 | 41 | 0.2469 | 3.94 | 6.90 |
| soccer2 | Soccer clip 2 | sports | 126 | 38 | 0.2270 | 3.89 | 7.58 |
| star | Star Wars | movie | 47 | 14 | 0.0842 | 4.02 | 13.40 |
| sbowl | Super Bowl | sports | 118 | 35 | 0.2125 | 3.01 | 5.99 |
| talk1 | Talk show | television | 73 | 22 | 0.1314 | 2.70 | 7.34 |
| talk2 | Political debate | television | 90 | 27 | 0.1620 | 3.21 | 7.41 |
| term | Terminator 2 | movie | 55 | 16 | 0.0986 | 3.11 | 7.30 |

These statistics provide a basic idea of the differences in the set of sample video streams. Of particular interest are the peak to average ratios measured at both the GOP and frame level. These values provide an estimate of the burstiness of a given video sequence [20] and indicate the potential for statistical multiplexing gain in the ATM network for each stream.

## 8. Traffic Simulations

In order to study the behavior of these video streams at the link between the multiplexor and the ATM network, three traffic simulation experiments were conducted. First, in order to better observe the effect of highly correlated video traffic on the network, a traffic simulation consisting of multiplexed traffic of 16 identical and synchronized video streams was designed. The traffic trace in Fig. 6 illustrates the character of the simulated traffic for approximately two minutes of the broadcast of the movie *Jurassic Park*.

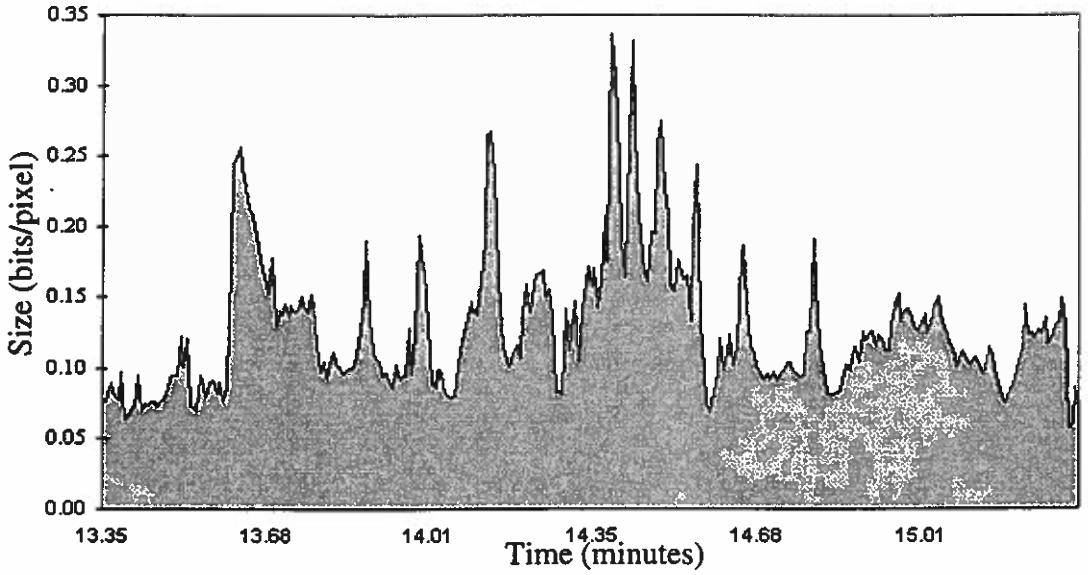


***Figure 6: 16 Synchronized* Jurassic Park *Traces***

As can be seen in Fig. 6, the multiplexed traffic is quite bursty, ranging from approximately 0.35 bits per pixel to about 0.07 bits per pixel. *Jurassic Park*'s average of 0.12 bits per pixel is greatly exceeded by the peaks in this graph, indicating potential difficulties for the network.

*Jurassic Park* was selected for this simulation because it displays some of the longer correlations of the sample group. Sixteen synchronized copies of the movie were broadcast to facilitate comparison with multiplexed traffic simulations consisting of one copy of each video stream in the sample group.

The second experiment used to measure the behavior of multiplexed MPEG traffic in the link differs only sightly from the first. In the second simulation, 16 copies of the same video sequence were again multiplexed and broadcast to the network. This time the video sequences were not synchronized. Instead, the start times of each video sequence were staggered 1.4 minutes from the previous start time (1.4 = 1/16 of the length of the entire video sequence).

By starting a new movie every 1.4 minutes and running them in a circular manner, 16 copies of the video were always multiplexed into the network traffic. As shown in Fig. 7, staggering the video streams in this manner reduces the burstiness of the resulting network traffic, despite

the fact that the video streams are identical and possess significant long-term correlations.

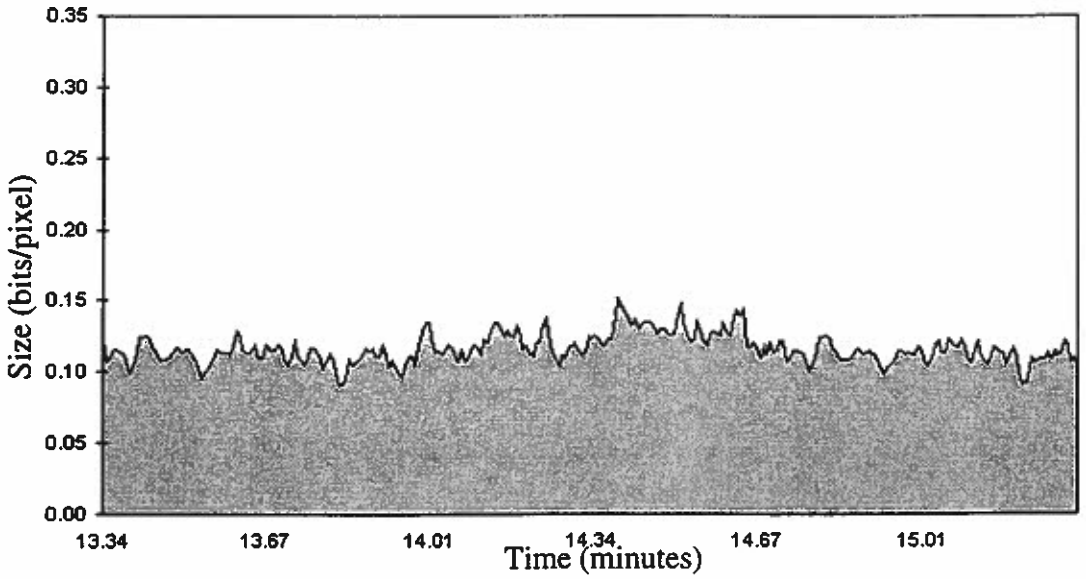


***Figure 7: 16 Staggered* Jurassic Park *Traces***

Comparing the traffic trace in Fig. 6 with that in Fig. 7 shows a significant decrease in burstiness when the start times are staggered. The same two minute portion of the video trace in Fig. 7 shows a range from approximately 0.15 bits per pixel to 0.09 bits per pixel while the trace in Fig. 6 ranges from 0.35 to 0.07 bits per pixel. Staggering the traces decreases the effects of the correlations in the video stream and yields smoother traffic.

To see how this result carries over to traffic which consists of different video sources, the third experiment is a traffic simulation of 16 independent video sequences. As in the first experiment, the video sequences of the third experiment have synchronized start times. However, each stream is different from the others. The trace in Fig. 8 illustrates the behavior of the simulated traffic of the third experiment.

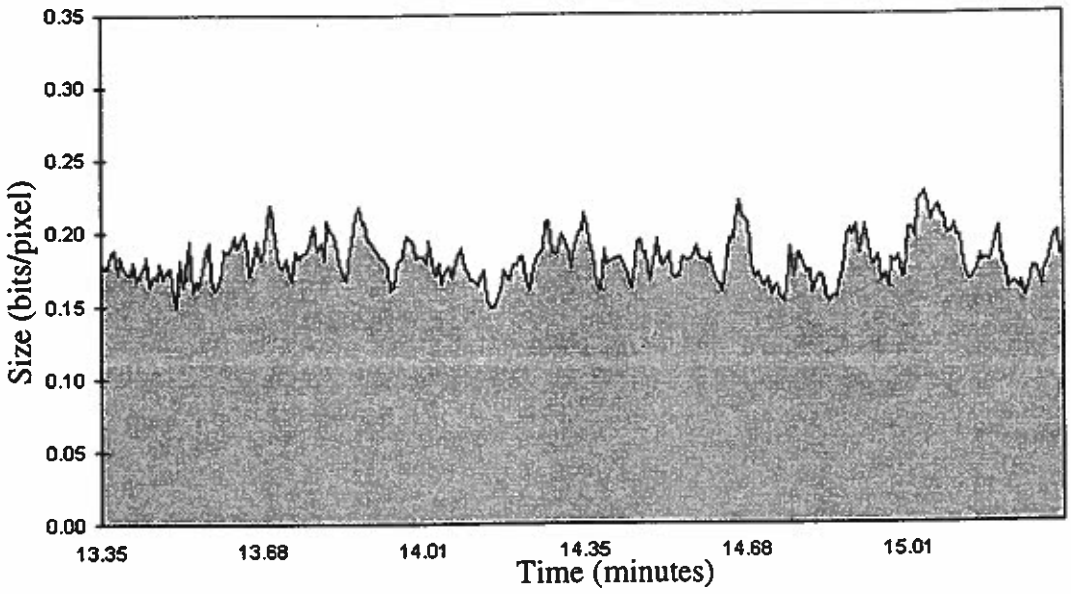


***Figure 8: 16 Different Synchronized Traces***

The traffic trace in Fig. 8 closely resembles the traffic trace in Fig. 7. There is little quantitative difference between the two traces. The trace of Fig. 8 yields a peak to average ratio of 2.4 while the trace of Fig. 7 yields a peak to average ratio of 2.0. The larger magnitude of the trace of Fig. 8 is attributable to the fact that Jurassic Park's average GOP size is one of the smallest in the sample set. The average of each of the three traces can be calculated from the characteristics of its component video streams.

When compared to the trace in Fig. 6, the trace in Fig. 8 exhibits relatively smooth behavior. Comparing the traces in Fig. 7 and Fig. 8, it can be observed that the long term correlations do not seem to be significant. In order to better study this correlation, however, it is useful to look at other measurements for each of the samples.

## 9. Autocorrelation Functions

One of the characteristic measurements used to describe video sequences is the autocorrelation function [20,21,33]. This function provides insight into the nature of any long term correlations which may exist in the video stream. When normalized by the variance, this function takes the form:

$$\rho(j) = \frac{E[(x(i)-\bar{x})(x(i+j)-\bar{x})]}{Var[x(i)]} \qquad \text{Eq. (1)}$$

For a stationary process, this yields an $R(j)$ dependent only on the lag $j$ and independent of the sampling time.

To evaluate each of the sixteen traces, the normalized autocorrelation function was fit to a single exponential. Plotting the curve which represents the single exponential fit with the normalized autocorrelation function shows that most of the traces exhibit a decay which cannot be expressed as a single exponential, as can be seen in the plot of the autocorrelation function of Jurassic Park in Fig. 9 below (and in the plots of Appendix C).

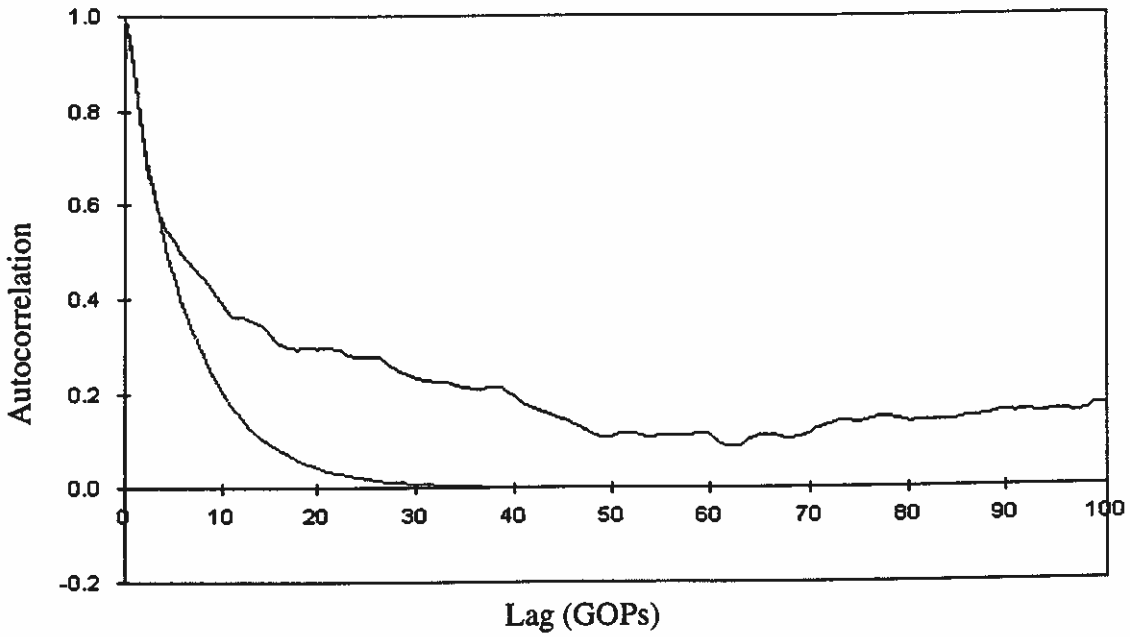


***Figure 9: Normalized Autocorrelation Function with Single Exponential Fit for* Jurassic Park**

Though not explicitly shown in Fig. 9, the autocorrelation of this trace and the others plotted in Appendix C have largely vanished after 1.4 minutes. Table 2 lists the decay constants for the single exponential approximation of the autocorrelation function for all sixteen traces.

**Table 2: Exponential Decay Constants for the 16 MPEG-1 Traces**

| Brief Name | Decay | Brief Name | Decay | Brief Name | Decay | Brief Name | Decay |
|---|---|---|---|---|---|---|---|
| ast | 0.8196 | mtv2 | 0.8193 | simp | 0.7232 | sbowl | 0.8648 |
| bond | 0.8804 | news1 | 0.8995 | soccer1 | 0.8257 | talk1 | 0.8981 |
| jp | 0.8538 | race | 0.8403 | soccer2 | 0.8378 | talk2 | 0.9284 |
| mtv1 | 0.7321 | lambs | 0.9094 | star | 0.8742 | term | 0.6835 |

To better understand the correlation effects of a single video sequence, double exponential curves were fit to the different autocorrelation functions. The general form of the double exponential fit was:

$$\rho(j) \equiv a\rho_1^j + (1-a)\rho_2^j \qquad \text{Eq. (2)}$$

For the fit of *Jurassic Park* shown in Fig. 10, $a = 0.716$, $\rho_1 = 0.854$ and $\rho_2 = 0.997$.

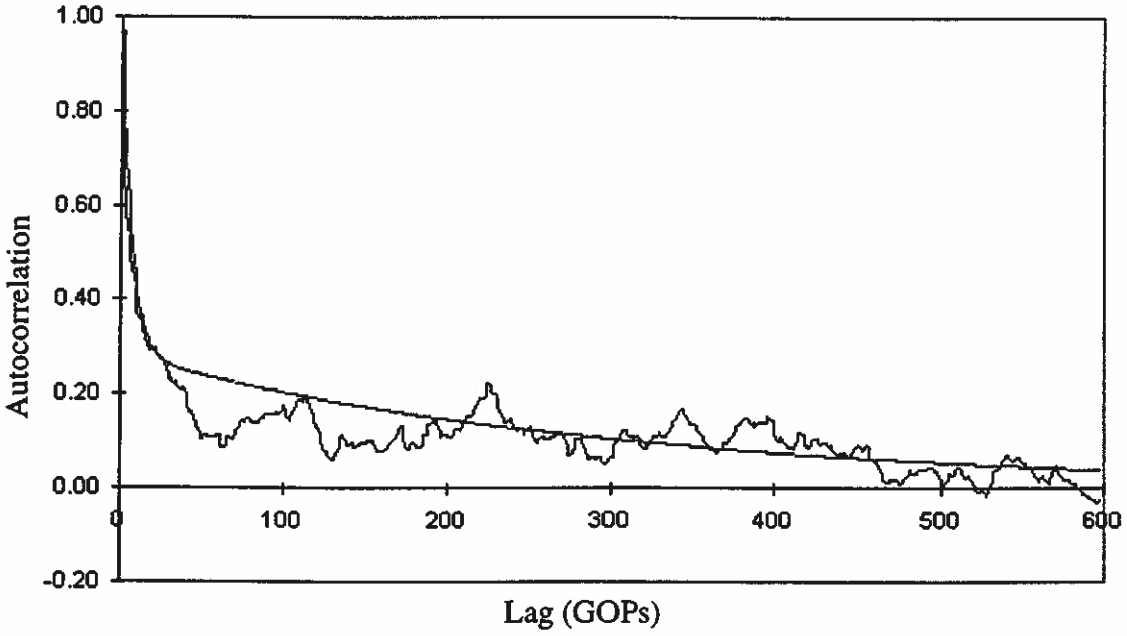


***Figure 10: Normalized Autocorrelation Function with Double Exponential Fit for* Jurassic Park**

Representing the autocorrelation function as a sum of exponents provides a significant benefit for video traffic modelling. If the autocorrelation function must be represented by a hyperbolic function, any resulting traffic models must conform to the requirements of self-similar statistics [32]. An approximation of the autocorrelation function can be made by taking the sum of a large number of exponentials [1]. However, if the double exponential fit proves to adequately approximate the autocorrelation function, traffic prediction calculations can be simplified significantly.

## 10. Proposed Traffic Model

Another method which is frequently used to illustrate long-term correlations in video sequences is the Variance-Time plot [32]. By plotting the variance against the number of GOPs aggregated together ($I$ in Eq. 3) using log-log axes, the independence, or lack thereof, in a data set can be observed. Plotted in this way, the variance-time plot of a statistically independent data set will have a slope of -1.0. Data sets exhibiting long-term dependency will have a slope less steep than -1.0.

Using the double exponential fit described in Section 9, a model of the variance-time plot of a video sequence can be derived. Using the same variables from the double exponential fit of

Eq.2, the model takes the form of:

$$\frac{\overline{m_k^2}}{\sigma_x^2} = \frac{a}{I}\left(\frac{1+\rho_1}{1-\rho_1} - \frac{2\rho_1}{I}\frac{1-\rho_1^I}{(1-\rho_1)^2}\right) + \frac{(1-a)}{I}\left(\frac{1+\rho_2}{1-\rho_2} - \frac{2\rho_2}{I}\frac{1-\rho_2^I}{(1-\rho_2)^2}\right) \quad \text{Eq. (3)}$$

where $\overline{m_k^2}$ is the variance of the sample means of all the aggregated GOPs in a sequence. The full derivation for this model is shown in Appendix A. The variables $a$, $\rho_1$ and $\rho_2$ are determined from the double exponential fit to the autocorrelation function.

In the plot of Fig. 11, the lower curve is the variance-time plot from the trace of GOP sizes for the *Jurassic Park* sequence. The upper curve is the proposed model defined by Eq. 3.

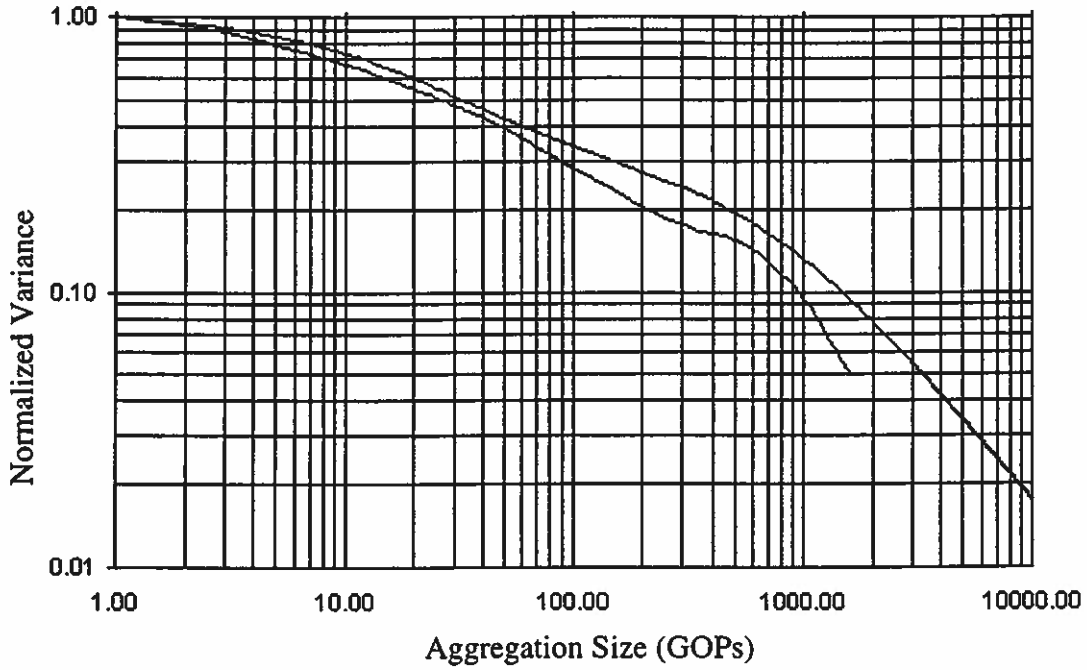


***Figure 11: Variance-Time Plot and Proposed Model for Jurassic Park***

An important observation which can be made concerning the plot in Fig. 11 is that the variance begins to fall linearly only after the aggregation size has reached 1000. At that point, the corresponding autocorrelation is below 0.1. Also, it should be noted that with only 3333 data points (the number of GOPs in the trace), as the aggregation size exceeds 1000 the data becomes unreliable. To see how well the model fits as the variance is falling linearly, larger sample sets are required.

As can be seen in Fig. 11, the model fits the experimental data reasonably well. This model will be especially useful in near-video-on-demand (NVOD) applications. In such applications, multiple copies of the same video are broadcast at regular intervals and long-term correlations between video sequences are possible since each broadcast is a time-shifted copy of a previous sequence. To determine how closely spaced in time such copies can be without losing any gain in statistical multiplexing, the model of Fig 11. can be used without having to rely on self-similar statistics. This approach leads to a simplification in the management of network traffic in

NVOD applications.

## 11. GOP Size Histograms

Another important characteristic of MPEG video traffic is its distribution. The histogram of the simulated traffic created from 16 different MPEG-1 traces, as shown in Fig. 4, provides important insight into the statistical nature of MPEG video traffic. By fitting the distribution to a number of different statistical distributions, it was observed that the distribution might fit most of the histogram very well while not adequately accounting for the entire histogram.

In looking at the different statistical distributions, it was observed that neither the Gaussian distribution nor the gamma distribution provides an adequate fit for the histogram of the experimental data [6,28]. However, the gamma distribution provides, for the most part, a very close approximation to the histogram of the simulated traffic. As shown in Fig. 12, the gamma distribution accounts for the behavior of the histogram reasonably well until the upper five or ten percent of the data.

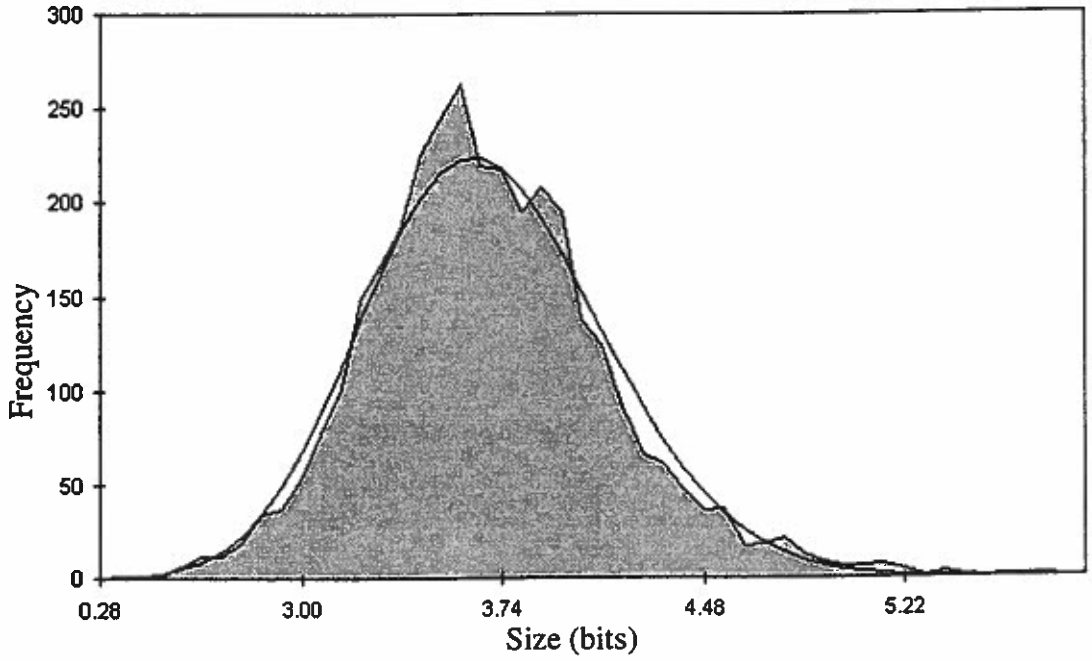


*Figure 12: GOP Size Histogram with Gamma Fit*

Since the gamma distribution cannot adequately account for the details of the tail, it becomes necessary to find another expression which can account for the long tail of the traffic. The primary reason this is important is that the tail of the histogram will be used to determine the bandwidth required at the multiplexor network link.

To better account for the slower decay of the tail a theoretical distribution was derived. From the derivation in Appendix B., it was found that the sum of the individual gamma distributions, representing each of the 16 video sequences leads to an expression for the tail which will be referred to as the gamma tail. As shown in Fig. 13, when compared to the tail of the gamma

distribution, the gamma tail expression provides a more conservative fit to the upper five percent of the traffic histogram when estimating bandwidth utilization.

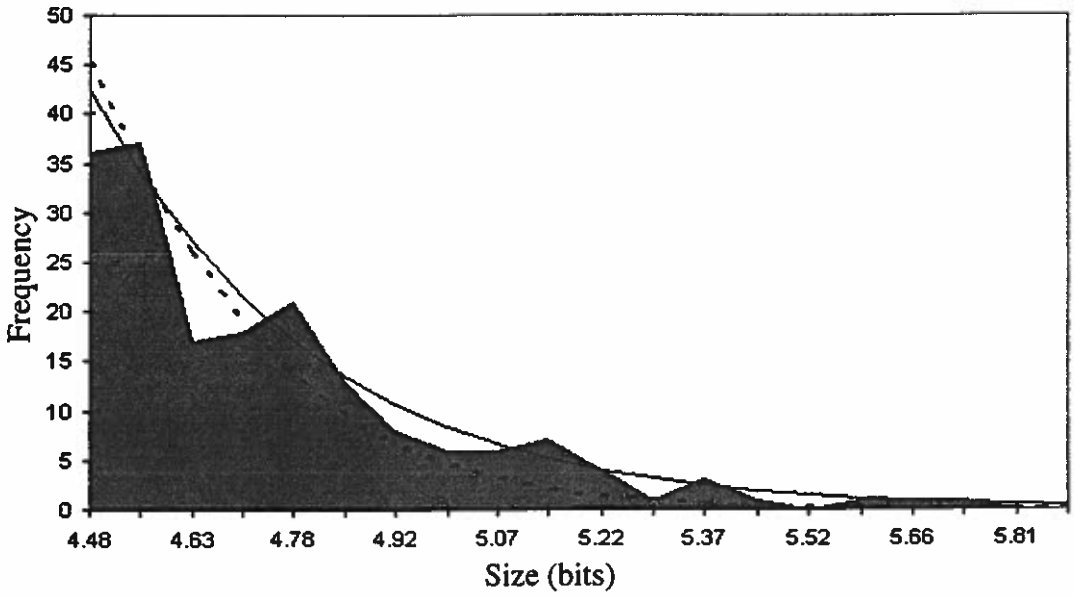


***Figure 13: Data, Gamma Distribution(dashed) and Gamma Tail(solid)***

The most important property of this representation of the traffic distribution is that the trace with the largest autocorrelation decay constant determines the expression of the gamma tail. Even though both the gamma distribution and the gamma tail are based on the gamma function, their curves are not identical because the gamma distribution is based on the mean and variance of all traces in the sample set while the gamma tail is based only on the mean and variance of the trace with the largest autocorrelation decay constant.

To predict the bandwidth required by the video traffic, it is necessary to know the autocorrelation decay constants, the mean, and the variance of each of the broadcast video sequences. It is then possible to calculate the tail of the traffic distribution using only these simple measurements to characterize the aggregate traffic sent to the link.

## 12. Link Bandwidth Utilization

Once the required bandwidth for the link has been calculated, it is necessary to determine the percentage of the bandwidth which can be utilized for video transmission. Because of the burstiness of VBR video sources, there will be periods of low bandwidth utilization. During these periods, network efficiency can be increased by filling in the remainder of the available bandwidth with ABR or best effort traffic. However, the degree of utilization will remain somewhat less than one hundred percent or else increases in the bandwidth required by the video traffic will cause an unacceptable increase in cell loss in the filler traffic.

To study the limits of bandwidth utilization another traffic simulation experiment was conducted. In this experiment, a certain bandwidth was requested based on the tail calculations described above. With this bandwidth requested, the video traffic was then given priority over the filler traffic. Two levels of bandwidth utilization were then set. One, shown in Fig. 14, was set at 90 percent. The second, shown in Fig. 15, was set at 95 percent.

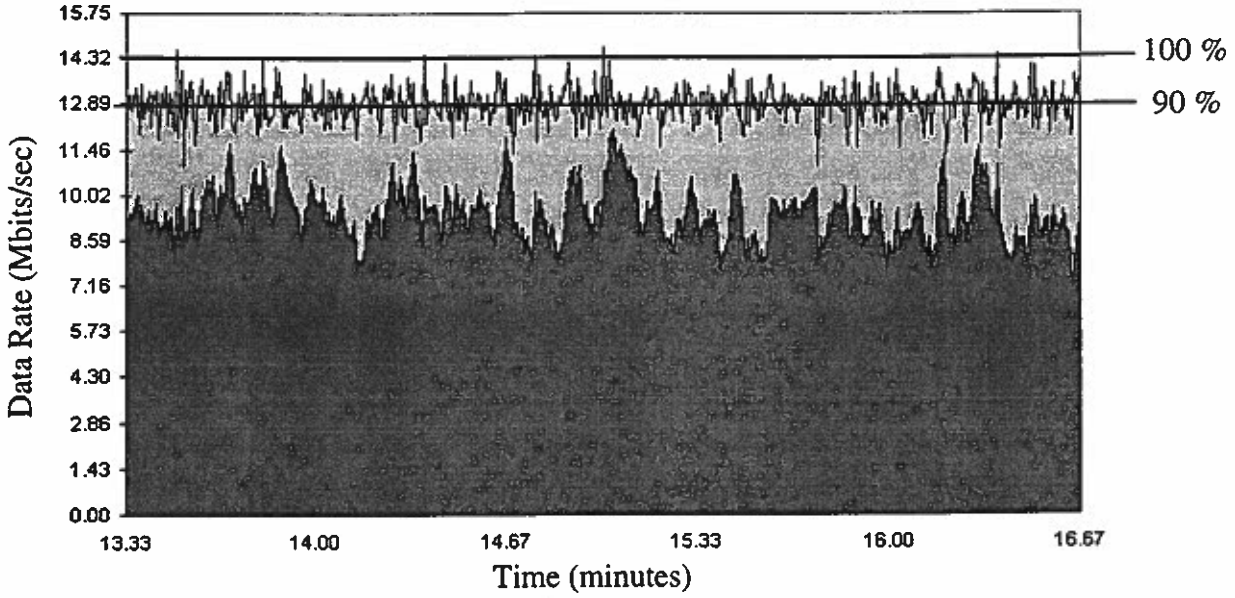


***Figure 14: 90% Bandwidth Utilization***

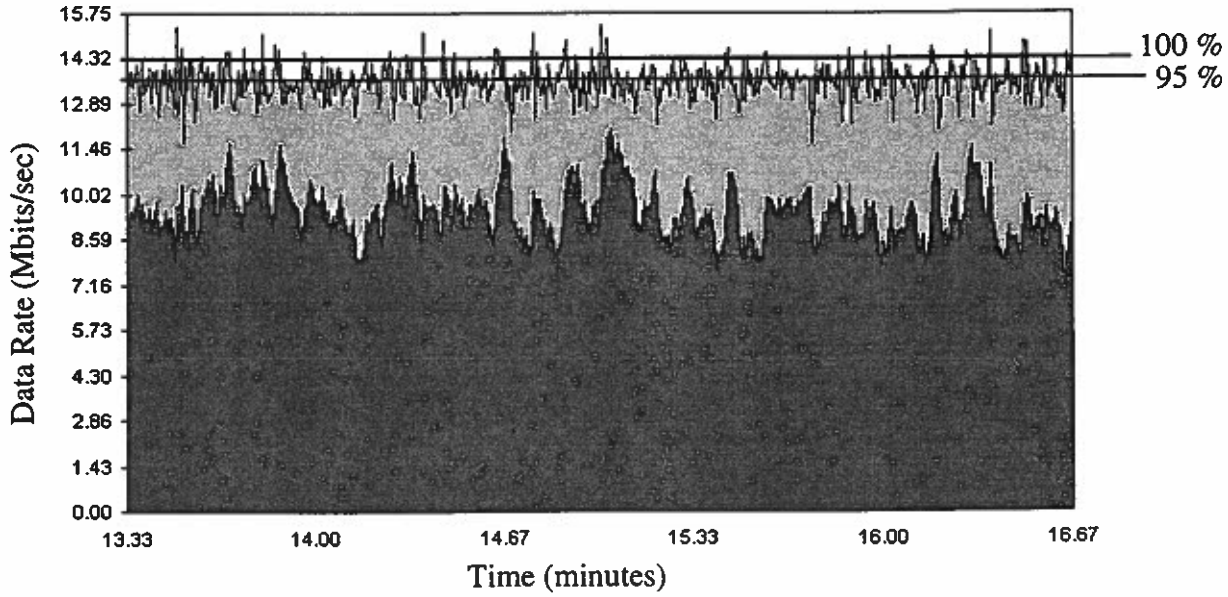


***Figure 15: 95% Bandwidth Utilization***

Cell loss occurs in both Fig. 14 and Fig. 15 any time either or both of the data types exceed the requested bandwidth calculated using the expression for the gamma tail, in this case, 14.32 Mbit/sec. As can be seen in Fig. 15, with the bandwidth utilization set at 95 percent in this

rough simulation, cell loss in the filler traffic becomes significant with over five percent of the peaks exceeding the requested bandwidth. Decreasing the bandwidth utilization to 90 percent greatly reduces the probability of cell loss, as shown in Fig. 14.

However, this may present an exaggerated estimation of the cell loss in the actual link, because of the nature of the two data types. Pacing the video data into the network at the GOP level means each data point will have a duration of approximately 0.4 seconds. Because of the higher temporal grain which can be achieved by the filler traffic, the cell loss shown as lasting 0.4 seconds will actually last a fraction of that, reducing the duration of overly large peaks.

Also, a number of more complex schemes can be employed to determine the amount of filler traffic to be sent in the next time segment. The scheme used for this simulation was especially crude. It simply set the filler rate for the next time slot equal to the difference between the available bandwidth at the current time and the current bandwidth required by the video sequence. With a response time of less than 0.4 seconds, the filler traffic can certainly do better than that.

## 13. Preliminary Cell Loss Model

To determine the degree of cell loss expected in the network, a preliminary cell loss model has been developed using the gamma tail model explained previously. Again, of primary importance is the fact that the component with the slowest decay (see Appendix B) controls the tail of the distribution of the aggregate traffic. This method allows for recalculation of required bandwidth any time a new movie starts or another movie finishes. The predicted cell loss and required bandwidth can then be calculated dynamically based on the video sequences currently being broadcast.

The effectiveness of this model in providing a conservative prediction of cell loss in MPEG video traffic can be observed from Fig. 16.

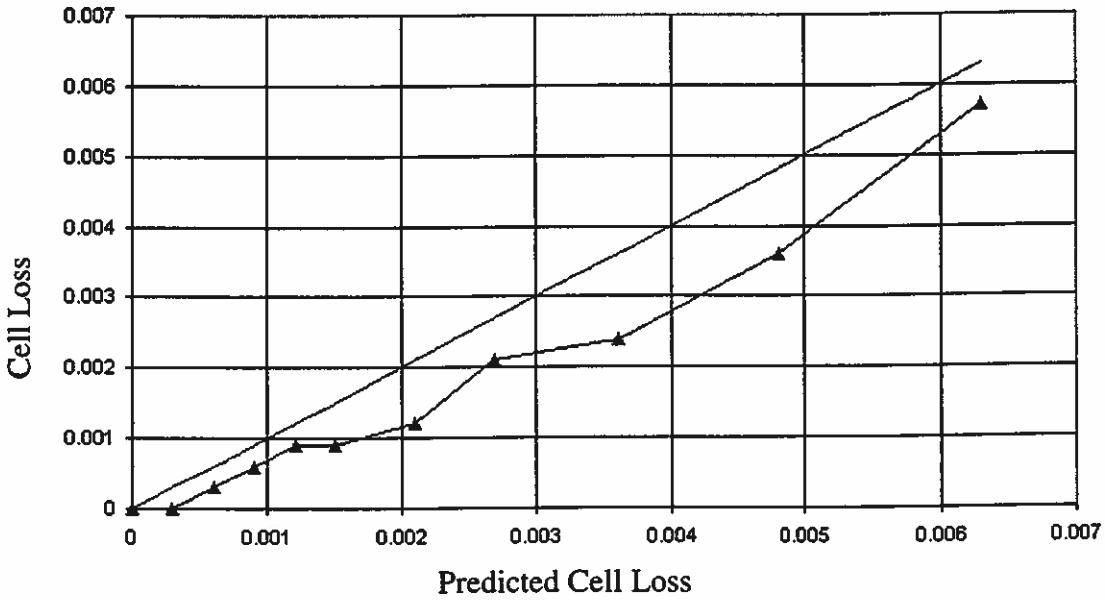


***Figure 16: Cell Loss Model***

In the above figure, the predicted cell loss is represented by the straight upper line. The cell loss resulting from offered load to the network that exceeds the bandwidth available is represented

by the lower line. For both lines, the horizontal axis is the predicted cell loss. If there were perfect agreement between the data and the model, the data points would fall on the predicted line. The fact that the predicted line is consistently higher than the data line indicates that the model provides a conservative estimate of the cell loss.

From Fig. 16 it is apparent that the model predicts cell loss reasonably well. Because of the limited sample set of this experiment, this preliminary result cannot be considered conclusive. To thoroughly test the effectiveness of this model it is important that it be evaluated with larger data sets and longer traffic simulations to see how well it behaves for a more representative sample group. Beyond MPEG-1 compressed video traffic, MPEG-2, JPEG and HDTV transmissions must be considered to determine the method's independence of codec type, picture size, and video sequence length.

## 14. Conclusion

During the course of this study, it has become clear that an effective way of incorporating MPEG video traffic into the ATM environment is to transmit MPEG video through the network as evenly paced, prioritized GOPs. ABR or best effort traffic can be used as filler traffic to increase bandwidth utilization without increasing the probability of cell loss in the MPEG traffic or incurring significant cell loss in the filler traffic. The degree of cell loss can be predicted using simple measurements from each of the component video sequences. With measurements of mean cell rate and variance for each of the component sequences, cell loss for the aggregate traffic can be accurately predicted. However, this study is by no means conclusive. Rather, it represents a preliminary development and must be tested against a much larger library of sample videos. This library must include video sequences encoded with a number of different VBR codecs and the video sequences must be of sufficient length to adequately study lags of thousands of GOPs. We believe this is a promising method which may significantly simplify VBR video modeling.

## A. Derivation of the Double Exponential Traffic Model

Given $x$, a random variable in the interval $[0,\infty)$ with a probability density $p(x)$; define a random process that is a sequence of consecutive samples of the random variable $x$ which we will call $x_i$ ($i$=0,1,2,3,...). The mean of the $i^{th}$ sample is

$$\bar{x}_i = \int_0^\infty x_i p(x_i)\, dx_i \tag{1}$$

and the covariance of the $i^{th}$ and $(i+j)^{th}$ sample is

$$R(i, i+j) = \overline{x_i x_{i+j}} = \int_0^\infty \int_0^\infty x_i x_{i+j} p(x_i, x_{i+j})\, dx_i dx_{i+j} \tag{2}$$

where $p(x_i, x_{i+j})$ is the joint density for the $i^{th}$ and $(i+j)^{th}$ samples. If we assume stationarity of the random process so that $\bar{x}_i = \bar{x}$ and $R(i, i) = \overline{x_i^2} = \overline{x^2}$, then

$$R(i, i+j) = \overline{(x_i - \bar{x} + \bar{x})\,(x_{i+j} - \bar{x} + \bar{x})} \tag{3}$$

$$R(i, i+j) = \overline{(x_i - \bar{x})\,(x_{i+j} - \bar{x})} + (\bar{x})^2 \tag{4}$$

$$R(i, i+j) = \rho(j)\,\sigma_x^2 + \bar{x}^2 \tag{5}$$

where $\rho(j)$ is the normalized autocorrelation function defined in Eq. 2 of Section 9.

$$\rho(j) \cong a\rho_1^j + (1-a)\,\rho_2^j \tag{6}$$

giving a decay which falls off exponentially with $j$ for each of the two terms that make up the approximation. Note that $\rho(0) = 1 = a + (1-a)$. Substituting the approximation into (5) we get

$$R(i, i+j) = a\rho_1^j \sigma_x^2 + (1-a)\,\rho_2^j \sigma_x^2 + \bar{x}^2 \tag{7}$$

If $x_i$ and $x_{i+j}$ were statistically independent

$$\overline{x_i x_{i+j}} = \bar{x}_i \overline{x_{i+j}} = \bar{x}^2; \qquad \rho(j) = \delta_{j0} \qquad \textit{and} \qquad \overline{x^2} = \sigma_x^2 + \bar{x}^2 \tag{8}$$

Given the sample mean:

$$m_k = \frac{1}{I} \sum_{i \in J_k} x_i \tag{9}$$

over $I$ samples in the $k^{th}$ group of $I$ samples such that $J_k = \{kI, kI+1, \ldots, (k+1)I-1\}$, the mean

squared value of the sample mean is

$$\overline{m_k^2} = \frac{1}{I^2}\sum_{i\in J_k}\sum_{l\in J_k}\overline{x_i x_l} = \frac{1}{I^2}\sum_{i\in J_k}\sum_{l\in J_k} R(i,l) = \frac{1}{I^2}\sum_{i\in J_k}\sum_{l\in J_k}\rho(i-l)\,\sigma_x^2 + \bar{x}^2 \qquad (10)$$

Where (5) has been used to introduce the normalized autocorrelation function, $\rho(i-l)$ and $l=i+j$. The double summation in (10) can be visualized as a real, $IxI$ square array in Toeplitz form. Utilizing the identity and symmetry of the elements along diagonals parallel to the array's major diagonal we can write

$$\overline{m_k^2} = \frac{\sigma_x^2}{I^2}\left[I\rho(0) + 2(I-1)\rho(1) + \ldots + 2\rho(I-1)\right] + \bar{x}^2$$

$$\overline{m_k^2} = \frac{2}{I^2}\sum_{j=0}^{I-1}(I-j)\,\rho(j)\,\sigma_x^2 - \frac{\sigma_x^2}{I} + \bar{x}^2 \qquad (11)$$

Now substituting for $\rho(j)\,\sigma_x^2$ from (6) and carrying out some straightforward summations for geometric series we get

$$\overline{m_k^2} = \frac{1}{I}\sum_{i=1}^{2}\sigma_{x_i}^2\left(\frac{1+\rho_i}{1-\rho_i} - \left(\frac{2\rho_i}{I}\right)\frac{1-\rho_i^I}{(1-\rho_i)}\right) + \bar{x}^2 \qquad (12)$$

where $\sigma_{x_1}^2 = a\sigma_x^2$ and $\sigma_{x_2}^2 = (1-a)\,\sigma_x^2$.

## B. Derivation of the GammaTail

The gamma probability density $p(n, \lambda, x)$ is defined as

$$p(n, \lambda, x) = \frac{\lambda (\lambda x)^{n-1} e^{-\lambda x}}{\Gamma(n)} \tag{1}$$

whose characteristic function $M(n, \lambda, u)$ is:

$$M(n, \lambda, u) = \frac{\lambda^n}{(\lambda - ju)^n} \tag{2}$$

Note that when $n$=1,

$$M(1, \lambda, u) = \frac{\lambda}{(\lambda - ju)} \tag{3}$$

and

$$\frac{\partial^{n-1} (M(1, \lambda, u)/\lambda)}{\partial \lambda^{n-1}} = \frac{\partial^{n-1} \left( \frac{1}{\lambda - ju} \right)}{\partial \lambda^{n-1}} = \frac{(-1)^{n-1}}{(\lambda - ju)^n} \Gamma(n) \tag{4}$$

Thus

$$M(n, \lambda, u) = \frac{-(-\lambda)^n}{\Gamma(n)} \frac{\partial^{n-1} (M(1, \lambda, u)/\lambda)}{\partial \lambda^{n-1}} \tag{5}$$

$$M(n, \lambda, u) = \frac{-(-1)^{2n-1} \lambda^n \Gamma(n)}{\Gamma(n) (\lambda - ju)^n} = \frac{\lambda^n}{(\lambda - ju)^n}$$

Similarly,

$$p(n, \lambda, x) = \frac{-(-\lambda)^n}{\Gamma(n)} \frac{\partial^{n-1} (p(1, \lambda, u)/\lambda)}{\partial \lambda^{n-1}} \tag{6}$$

$$p(n, \lambda, x) = \frac{-(-\lambda)^n}{\Gamma(n)} \frac{\partial^{n-1} e^{-\lambda x}}{\partial \lambda^{n-1}} = \frac{\lambda (\lambda x)^{n-1} e^{-\lambda x}}{\Gamma(n)}$$

Now consider $s = \sum_{i=0}^{I-1} x_i$ where the $x_i$ are statistically independent. Then the characteristic function for the $s$ is

$$M(\underline{n}, \underline{\lambda}, u) = \prod_{i=0}^{I-1} M(n_i, \lambda_i, u) = \prod_{i=0}^{I-1} \frac{\lambda_i^{n_i}}{(\lambda_i - ju)^{n_i}} \tag{7}$$

Let us assume that the $\lambda_i$ are distinct and increasing $(\lambda_0 < \lambda_1, \ldots, \lambda_{n_i - 1} < \lambda_{n_i})$. Furthermore, expand the characteristic function into partial fractions

$$M(\underline{n}, \underline{\lambda}, u) = \sum_{i=0}^{I-1} \sum_{j=1}^{n_i} \frac{a_{ij} \lambda_i^j}{(\lambda_i - ju)^j} \tag{8}$$

The probability density for the sum $s$ becomes

$$p(\underline{n}, \underline{\lambda}, s) = \sum_{i=0}^{I-1} \sum_{j=0}^{n_i} a_{ij} \lambda_i \frac{(\lambda_i s)^{j-1} e^{-\lambda_i s}}{\Gamma(j)} \tag{9}$$

In the right-hand tail $(s \to \infty)$ only the term with the smallest $\lambda_i$, (i.e. $\lambda_0$) which also has the largest $j$ (i.e. $n_0$) will predominate. Thus,

$$\lim_{s \to \infty} p(\underline{n}, \underline{\lambda}, s) = a_{0n_0} \lambda_0 \frac{(\lambda_0 s)^{n_0 - 1} e^{-\lambda_0 s}}{\Gamma(n_0)} \tag{10}$$

where

$$a_{0n_0} = \lim_{ju \to \lambda_0} \left[ \left( \frac{\lambda_0 - ju}{\lambda_0} \right)^{n_0} M(\underline{n}, \underline{\lambda}, u) \right] = \prod_{i=1}^{I-1} \left( \frac{\lambda_i}{\lambda_i - \lambda_0} \right)^{n_i} \tag{11}$$

Note that $\lambda_i = \frac{\bar{x}_i}{\sigma_i^2}$ and $n_i = \left( \frac{\bar{x}_i}{\sigma_i} \right)^2$ so $a_{0n_0}$ and the tail probability density can be evaluated from the first two moments of the component distributions.

## C. Autocorrelation Plots for the 16 Samples

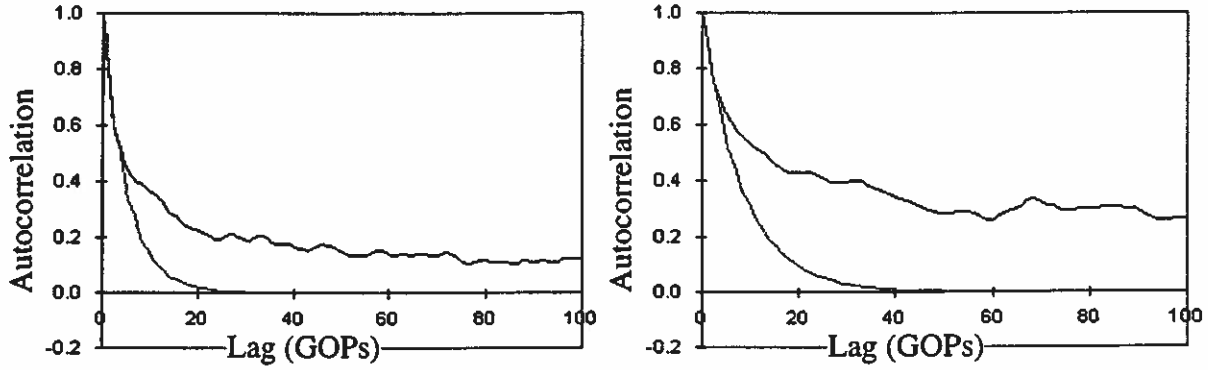


*Figure 1C: Autocorrelation Plots for ast (l) and bond (r)*

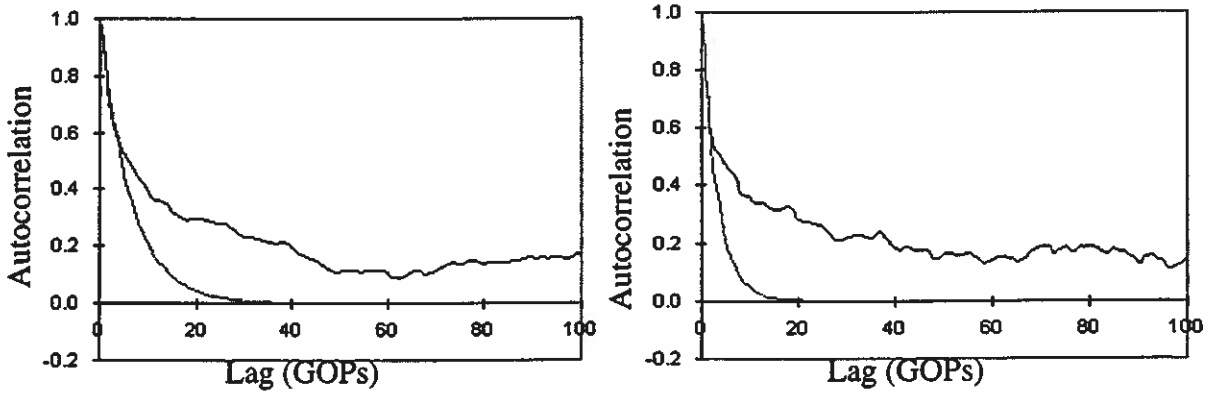


*Figure 2C: Autocorrelation Plots for jp (l) and mtv1 (r)*

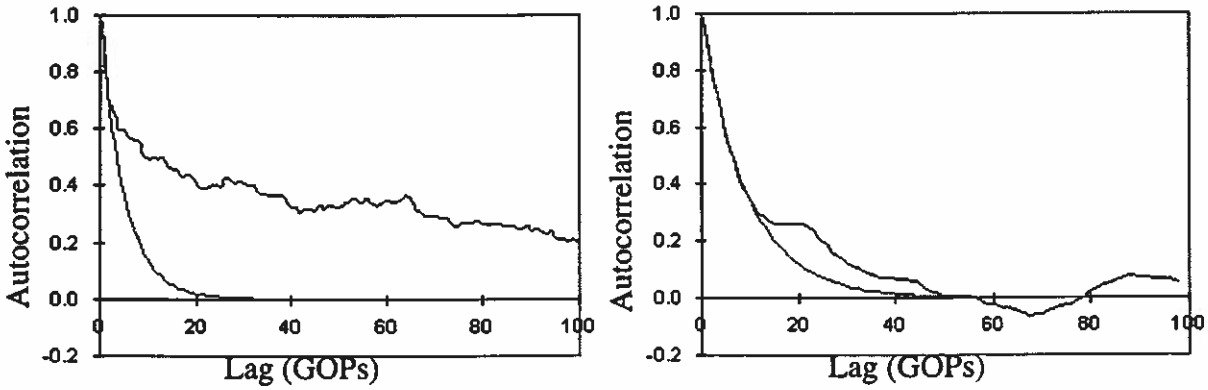


*Figure 3C: Autocorrelation Plots for mtv2 (l) and news1 (r)*

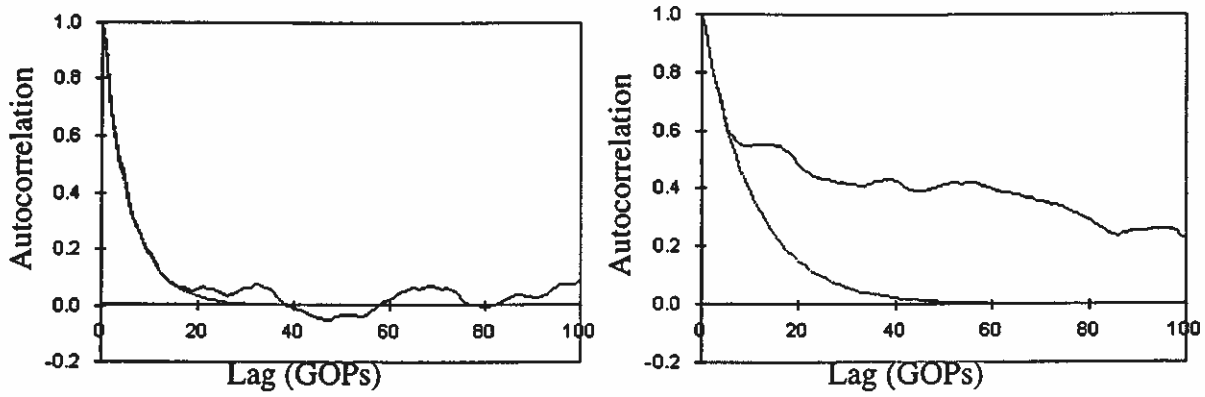


***Figure 4C: Autocorrelation Plots for race (l) and lambs (r)***

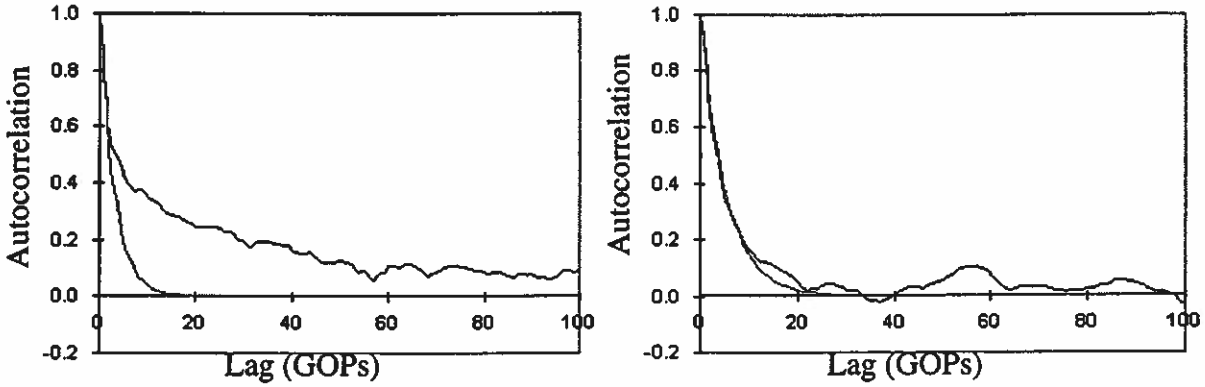


***Figure 5C: Autocorrelation Plots for simp (l) and soccer (r)***

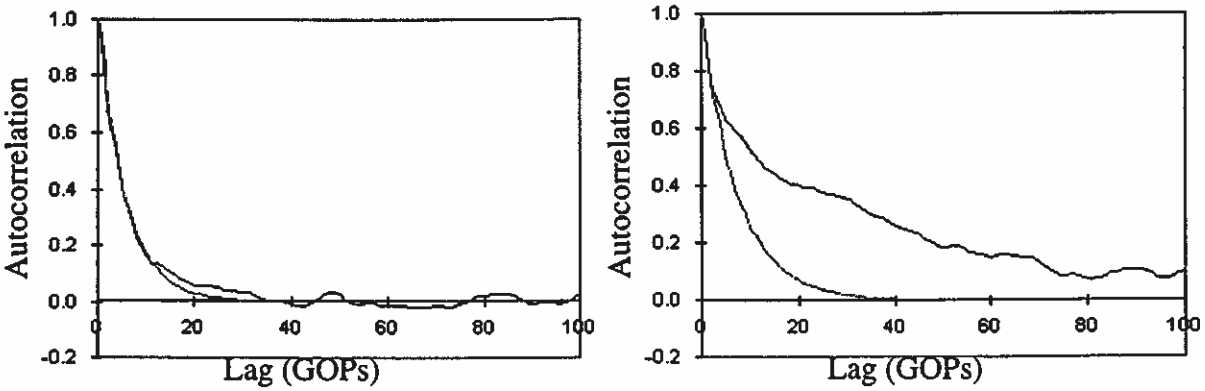


***Figure 6C: Autocorrelation Plots for soccer2 (l) and star (r)***

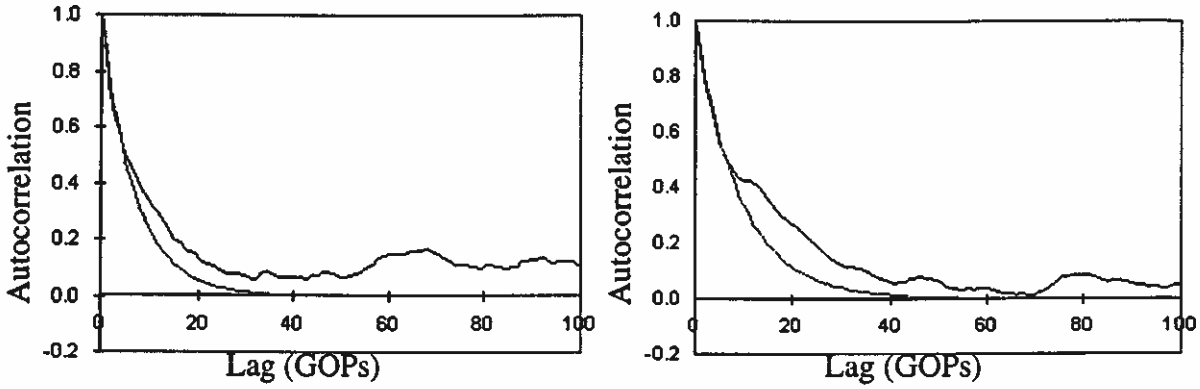


***Figure 7C: Autocorrelation Plots for sbowl (l) and talk1 (r)***

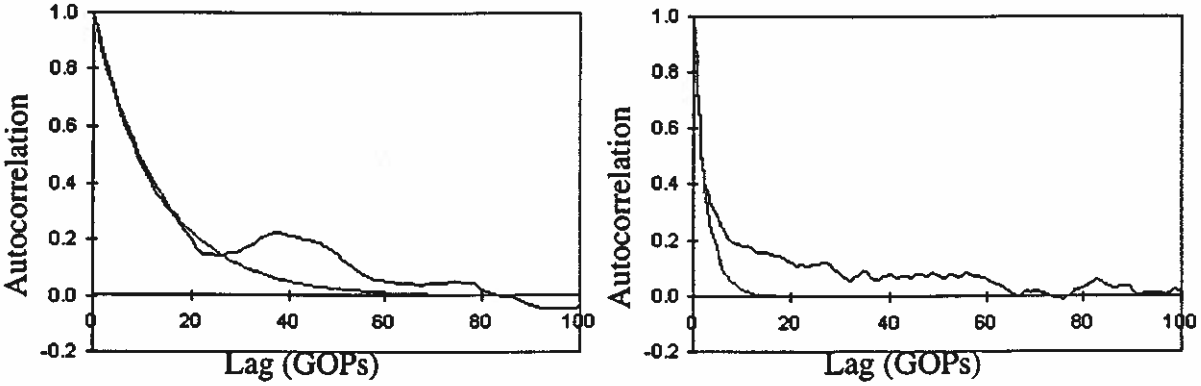


***Figure 8C: Autocorrelation Plots for talk2 (l) and term (r)***

## References


[1] J. Beran, R. Sherman, M. S. Taqqu, W. Willinger, "Long-Range Dependence in Variable-Bit-Rate Video Traffic," *IEEE Transactions on Communications*, Vol. 43, No. 2/3/4, Feb./Mar./Apr. 1995, pp. 1566-1579.

[2] H. S. Chin, J. W. Goodge, R. Griffiths, D. J. Parish, "Statistics of Video Signals for Viewphone-Type Pictures," *IEEE Journal on Selected Areas in Communications*, Vol. 7, No. 5, June 1989, pp. 826-832.

[3] S. Chong, S.-Q. Li, J. Ghosh, "Dynamic Bandwidth Allocation for Efficient Transport of Real-Time VBR Video over ATM," *Proceedings IEEE Infocom '94*, Toronto, Canada, June 1994, pp. 81-90.

[4] A. Erramilli, "Performance Impacts of Self-Similarity in Traffic," Performance evaluation review: a quarterly publication of the Special Interest Committee on Measurement and Evaluation, Vol. 23, 1995, pp. 265-266.

[5] B. Fuhrt, "Multimedia Systems: An Overview," *IEEE Multimedia*, Vol. 1, No. 1, Spring 1994, pp. 47-59.

[6] M. W. Garrett, W. Willinger, "Analysis, Modeling and Generation of Self-Similar VBR Video Traffic," *Proc. ACM SIGComm '94*, London, UK, 1994, pp. 269-280.

[7] D. P. Heyman, A. Tabatabai, T. V. Lakshman, "Statistical Analysis and SImulation Study of Video Teleconference Traffic in ATM Networks," *IEEE Transactions on Circuits and Systems for Video Technology*, Vol. 2, No. 1, March 1992, pp. 49-59.

[8] D. P. Heyman, A. Tabatabai, T. V. Lakshman, "Statistical Analysis of MPEG-2 Coded VBR Video Traffic," *Sixth International Workshop on Packet Video*, September 26-27, 1994, pp. B2.1-B2.5.

[9] ISO/IEC 11172, Information Technology - Coding of moving pictures and associated audio for digital storage media up to 1.5 Mbit/s.

[10] ISO/IEC 13818, Information Technology - Coding of moving pictures and associated audio information.

[11] G. Karlsson, M. Vetterli, "Packet Video and Its Integration into the Network Architecture," *IEEE Journal on Selected Areas in Communications*, Vol. 7, No. 5, June 1989, pp. 739-751.

[12] T. Koga, Y. Iijima, K. Iinuma, T. Ishiguro, "Statistical Performance Analysis of an Interframe Encoder for Broadcast Television Signals," *IEEE Transactions on Communications*, Vol. Com-29, No. 12, December 1981, pp. 1868-1875.

[13] D. J. LeGall, "MPEG: A Video Compression Standard for Multimedia Applications," *Communications of the ACM*, Vol. 34, No. 4, April 1991, pp. 47-58.

[14] D. J. LeGall, "The MPEG Video Compression Algorithm," *Signal Processing: Image Communication*, Vol. 4, No. 2, April 1992, pp. 129-140.

[15] S.-Q. Li, "A General Solution Technique for Discrete Queueing Analysis of Multimedia Traffic on ATM," *IEEE Transactions on Communications*, Vol. 39, No. 7, July

1991, pp. 1115-1132.

[16] S.-Q. Li, H.-D. Sheng, "Discrete Queueing Analysis of Multi-Media Traffic with Diversity of Correlation and Burstiness Properties," *Proceedings IEEE Infocom '91*, Bal Harbour, FL USA, April 1991, pp. 368-381.

[17] F. Kishino, K. Manabe, Y. Hayashi, H. Yasuda, "Variable Bit-Rate Coding of Video Signals for ATM Networks," *IEEE Journal on Selected Areas in Communications*, Vol. 7, No. 5, June 1989, pp. 801-806.

[18] B. Maglaris, D. Anastassiou, P. Sen, G. Karlsson, J. D. Robbins, "Performance Models of Statistical Multiplexing in Packet Video Communications," *IEEE Transactions on Communications*, Vol. 36, No. 7, July 1988.

[19] N. M. Marafih, Y.-Q. Zhang, R. L. Pickholtz, "Modeling and Queueing Analysis of Variable-Bit-Rate Coded Video Sources in ATM Networks," *IEEE Transactions on Circuits and Systems for Video Technology*, Vol. 4, No. 5, April 1994, pp. 121-127.

[20] A. N. Netravali, B. G. Haskell, *Digital Pictures: Representation, Compression, and Standards*, 2nd ed., New York: Plenum Press, 1995.

[21] M. Nomura, T. Fujii, N. Ohta, "Basic Characteristics of Variable Rate Video Transmission," *IEEE Journal on Selected Areas in Communications*, Vol. 7, No. 5, June 1989, pp. 752-760.

[22] N. Ohta, *Packet Video: Modeling and Signal Processing*, Norwood, MA.: Artech House, Inc., 1994.

[23] P. Pancha, M. El Zarki, "Bandwidth-Allocation Schemes for Variable-Bit-Rate MPEG Sources in ATM Networks," *IEEE Transactions on Circuits and Systems for Video Technology*, Vol. 3, No. 3, June 1993, pp. 190-198.

[24] P. Pancha, M. El Zarki, "MPEG Coding for Variable Bit Rate Video Transmission," *IEEE Communications Magazine*, May 1994, pp. 54-66.

[25] V. Paxson, S. Floyd, "Wide Area Traffic: The Failure of Poisson Modeling," *IEEE/ACM Transactions on Networking*, Vol. 3, No. 3, June 1995, pp. 226-244.

[26] A. R. Reibman, B. G. Haskell, "Constraints on Variable Bit-Rate Video for ATM Networks," *IEEE Transactions on Circuits and Systems for Video Technology*, Vol. 2, No. 4, December 1992, pp. 361-372.

[27] A. R. Reibman, A. W. Berger, "Traffic Descriptors for VBR Video Teleconferencing Over ATM Networks," *IEEE/ACM Transactions on Networking*, Vol. 3, No. 3, June 1995, pp. 329-339.

[28] O. Rose, "Statistical properties of MPEG video traffic and their impact on traffic modelling in ATM systems," *University of Wuerzburg Institute of Computer Science Research Report Series*, Report No. 101, Feb. 1995, pp. 1-25.

[29] P. Sen, B. Maglaris, N.-E. Rikli, D. Anastassiou, "Models for Packet Switching of Variable-Bit-Rate Video Sources," *IEEE Journal on Selected Areas in Communications*, Vol. 7, No. 5, June 1989, pp. 865-869.

[30] P. J. van der Meer, J. Biemond, R. L. Lagendijk, "Modeling and Multiplexing of VBR

Video without Network Constraints," *Sixth International Workshop on Packet Video*, Sept. 26-27, 1994, pp. D8.1-D8.4.

[31] W. Verbiest, L. Pinnoo, B. Voeten, "The Impact of the ATM Concept on Video Coding," *IEEE Journal on Selected Areas in Communications*, Vol. 6, No. 9, December 1988, pp. 1623-1632.

[32] I. Wakeman, "Packetized Video -- Options for Interaction between the User, the Network and the Codec," *The Computer Journal*, Vol. 36, No. 1, 1993, pp. 55-66.

[33] W. Willinger, M. S. Taqqu, W. E. Leland, D. V. Wilson, "Self-Similarity in High-Speed Packet Traffic: Analysis and Modeling of Ethernet Traffic Measurements," *Statistical Science*, Vol. 10, No. 1, 1995, pp. 67-85.

[34] F. Yegenoglu, B. Jabbari, Y.-Q. Zhang, "Motion Classified Autoregressive Modeling of Variable Bit Rate Video," *IEEE Transactions on Circuits and Systems for Video Technology*, Vol. 3, No. 1, February 1993, pp. 42-53.

[35] Y.-Q. Zhang, W. W. Wu, K. S. Kim, R. L. Pickholtz, J. Ramasastry, "Variable Bit-Rate Video Transmission in the Broadband ISDN Environment," *Proceedings of the IEEE*, Vol. 79, No. 2, February 1991, pp. 214-221